Detecting Attomolar DNA-Damaging Anticancer Drug Activity in Cell Lysates with Electrochemical DNA Devices

*Ashan Wettasinghe,[a] Naveen Singh,[b,c] Colton L. Starcher,[b] Chloe C. DiTusa,[a] Zakari Ishak-Boushaki,[a] Dimithree Kahanda,[a,d] Reema McMullen[a] Edward A. Motea,[b] and Jason D. Slinker[a,e]**

[a]Department of Physics, The University of Texas at Dallas, 800 W. Campbell Rd., SCI 10, Richardson, TX 75080 USA

[b]Department of Biochemistry and Molecular Biology, Simon Comprehensive Cancer Center, 980 W. Walnut Street, Walther Hall R3 C551, Indiana University School of Medicine, Indianapolis, IN 46202 USA

[c]Current Address: Department of Chemistry, New Mexico Highlands University, Box 9000, Las Vegas, NM 87701-9000 USA

[d]Department of Physics, University of Peradeniya, Peradeniya, Sri Lanka.

[e]Department of Materials Science and Engineering, The University of Texas at Dallas, 800 W. Campbell Rd., SCI 10, Richardson, TX 75080 USA

* slinker@utdallas.edu; 1-972-883-6513

Abstract

Here we utilize electrochemical DNA devices to quantify and understand the cancer-specific DNA-damaging activity of an emerging drug in cellular lysates at femtomolar and attomolar concentrations. Isobutyl-deoxynyboquinone (IB-DNQ), a potent and tumor-selective NAD(P)H quinone oxidoreductase 1 (NQO1) bioactivatable drug, was prepared and biochemically verified in cancer cells highly expressing NQO1 (NQO1+) and knockdowns with low NQO1 expression (NQO1−) by Western Blot, NQO1 activity analysis, survival assays, oxygen consumption rate, extracellular acidification rate, and peroxide production. Lysates from these cells and IB-DNQ drug were then introduced to a chip system bearing an array of DNA modified electrodes, and their DNA-damaging activity quantified by changes in DNA-mediated electrochemistry arising from base-excision repair. Device-level controls of NQO1 activity and kinetic analysis were used to verify and further understand IB-DNQ activity. A 380 aM IB-DNQ limit of detection and a 1.3 fM midpoint of damage was observed in NQO1+ lysates, both metrics two orders of magnitude lower than NQO1− lysates, indicating high IB-DNQ potency and selectivity for NQO1+ cancers. The device-level damage activity in lysates was over eight orders of magnitude lower than cell survival benchmarks, likely due to poor IB-DNQ cellular uptake, demonstrating that these devices can identify promising drugs requiring improved cell permeability. Ultimately, these results speak to the noteworthy potency and selectivity of IB-DNQ and the high sensitivity and precision of electrochemical DNA devices to analyze agents/drugs involved in DNA-damaging chemotherapies.

Keywords: electrical biosensor; oxidative damage; square wave voltammetry; base-excision repair; β-lapachone; IB-DNQ; NQO1-bioactivatable drugs; toxicology

DNA-damaging chemotherapies are extensively used to treat cancer and disease.[1-3] Current therapies such as cisplatin, methotrexate, and doxorubicin leverage DNA damage, as well as several emerging treatments.[1] Given the developing landscape of DNA-damaging drugs and the complexity of biological samples, it would be highly beneficial to develop sensors that can follow drug activity under biological conditions to efficiently identify promising drugs that target cancer while producing minimal side effects. Even so, it can be challenging to predict how a drug will impact a patient, given the wide range of damage repair pathways in the body and the variation of individual therapeutic responses.[4] Electrical biosensors are a safe and effective way of estimating DNA damage by promising new drugs targeting DNA or screening the safety of chemicals and carcinogens for potential toxicity. This novel testing paradigm is in line with the 3Rs (replacement, refinement, and reduction of animals in research) for existing regulatory frameworks to minimise animal use in the initial screening process of viable drug candidates.

Electrochemical devices are at the forefront of emerging biotechnologies and biological detection strategies.[5-9] They have been used in the biological detection of the heart drug digoxin, [10] recreational drugs such as cocaine,[11-12] the metabolic agent insulin,[13] the pain medications diclofenac and acetaminophen,[14] the anticancer drug doxorubicin,[15] and others.[16] We recently leveraged electrochemical DNA devices to follow DNA damage responses to anticancer drug treatment in lysates of cancerous and normal cells.[17] Gold electrodes patterned on devices were modified with clusters of synthetic DNA bearing an electrochemical probe. Under a negative bias, where the DNA is repelled from the surface, an electrical current reaches the probe only if the DNA remained fully intact, but transport is lost if the DNA was structurally compromised by damage or damage repair responses.[18-21] Nuclei were removed from cells, and both the nuclear and remaining cytoplasmic components were lysed and added onto the chips modified with DNA.

Anticancer drugs were added to this solution over the device, and the synthetic DNA on the chip recorded damage responses. The anticancer drug β-lapachone was shown to produce selective DNA damage as much as 3.7 times higher for NQO1+ cancerous cell lysates versus control (Kahanda et al. 2018). Mechanistic controls of drug activity were verified, and the concentration dependence of DNA damage on the chip was shown to correlate with critical points of drug-induced cell death.

Here we utilize electrochemical DNA devices to explore the emerging DNA-damaging anticancer drug, isobutyl-deoxynyboquinone (IB-DNQ).[22] In cell survival assays, IB-DNQ and associated derivatives are 6-100 times more potent than β-lapachone and yield higher selectivity.[23-26] However, the underlying DNA-damaging activity of this drug has yet to be systematically explored in a biological environment, and its higher potency offers the potential to investigate the sensitivity limits of electrochemical DNA device technology. This study thoroughly investigates the concentration dependence, selectivity, and mechanism of the IB-DNQ drug and discusses the factors enabling high precision biosensing of its activity with electrochemical DNA devices.

Experimental Section

Cell Culture, Chemicals, and Reagents. MDA-MB- 231 cells (231 hereafter) were obtained from American Tissue Culture Collection (ATCC, Manassas, VA). *NQO1-*2* polymorphic human MDA-MB-231 triple-negative breast and genetically matched NQO1+ cancer cells were generated as described elsewhere.[17,24] Isobutyl-deoxynyboquinone (IB-DNQ) was provided by the Boothman and Hergenrother lab and synthesized as described.[27] Catalase and dicoumarol were purchased from Sigma-Aldrich (St Louis, MO). All quinones were dissolved in dimethyl sulfoxide (DMSO). Cytoplasmic and Nuclear extracts from cell lines were prepared according to the

manufacturer's instructions (NE-PER™ Nuclear and Cytoplasmic Extraction Reagents, Cat. No. 78833, Thermo Scientific, Waltham, MA).

Western Blot analysis and NQO1 Enzyme Activity Assays. Western Blot measurements were performed as previously described.[17] NQO1 enzyme activities for the cell lines were measured as dicoumarol-inhibited units as described elsewhere.[28] Human NQO1 antibody was provided by Dr. David Ross (University of Colorado Health Science Center, Denver, CO) and used at a 1:1000 dilution overnight, 4 °C. α-Tubulin (Santa-Cruz Biotechnology, Dallas, TX), a house-keeping antibody, was used at 1:5000 dilution as a loading control.

DNA Survival Assays. Using NQO1+ and NQO1− 231 cells, relative survival assays were recorded as previously described.[17] Cells were plated into a 48-well plate with 10,000 cells/well in 500 μL of DMEM containing 10% FBS. The cells were allowed to attach and grow overnight. Drug concentrations (0 – 0.4 μM) were prepared separately in 15 mL conical tubes. The untreated control was DMSO. The media was removed from each well, and 500 μL of each drug concentration was added to 6 wells (to produce sextuplet replicates for each concentration). The plates were gently shaken to mix and placed in the incubator for 2 h. After 2 h, all media was aspirated from the wells, and 1 mL of fresh media was aliquoted into each well. The plates were then left in the incubator for 7 days or until there was 100% confluency for the untreated control. Once the control was confluent, the media was discarded, and 500 μL/well of 1X PBS was added to wash the wells. The PBS was discarded, and 250 μL of dH_2O/well was added. The plates were then put in a −80 °C freezer overnight. The next day, the plates were thawed completely, and 500 μL of Hoechst staining buffer (50 μL of Hoechst 33258 in 50 mL of 1X TNE buffer) was added to each well. The plates were incubated in the dark at RT for 2 h. After two hours, the plates were

read on a PerkinElmer Victor X3 plate reader, and the readings were plotted as the treated/control (T/C) ± SEM. Results were reported as means ± standard error (SE) from at least three independent experiments done in sextuplicate.

Analysis of Oxygen Consumption Rate (OCR) and Extracellular Acidification Rate (ECAR). The Seahorse XF96 Extracellular Flux Analyzer (Seahorse Bioscience, North Billerica, MA) was used to assess real-time *Oxygen Consumption Rate (OCR),* an indicator of mitochondrial respiration, and extracellular acidification rate (ECAR), an indicator of net proton loss during glycolysis *in* NQO1+ and NQO1− 231 cell lines upon IB-DNQ treatment. Before the start of the experiment, cells were evenly seeded (3,000 cells/well) into the 96-well XF96 cell culture plate and allowed to attach for 24 hours. A calibration plate was also prepared according to the manufacturer's instructions by placing it in a non-CO_2 37°C incubator. After prior washing with XF media, cell culture media was replaced with XF media (Seahorse Bioscience), lacking sodium bicarbonate and FBS. Cells were placed in a non-CO_2 37°C incubator for 1 hour before starting the experiment. Following the establishment of a basal OCR reading, OCR and ECAR were measured with IB-DNQ addition. OCR and ECAR readings were normalized to total protein levels (BCA protein assay, Pierce) in each well. Each cell line was represented in 6 wells per experiment, and replicate experiments were carried out at least three times.

H_2O_2 Measurements. Hydrogen peroxide (H_2O_2) (ROS-Glo) levels were assayed at indicated concentrations and time-points during treatments as indicated using specific assays previously developed and as described in the manufacturer's protocol (Promega ROS-Glo H_2O_2 Assay, Promega, Madison, WI). Two-way ANOVA and multiple t-tests were used for statistical analyses using GraphPad PRISM 7.05. The assay was performed in three biological replicates.

Synthesis of Oligonucleotides. The DNA used on the chip surfaces were the 17mer sequence 3'-CTC TAT ATT TCG TGC G(T_{NB})-5' and the fully complementary sequence 5′-(C_6 thiol)-GAG ATA TAA AGC ACG CA-3′, where T_{NB} is the Nile Blue modified thymine, and C_6 thiol is a 6-carbon alkanethiol. The thiolated oligonucleotide sequence was obtained from Integrated DNA Technologies (IDT). The DNA containing the Nile blue precursor base was purchased from Trilink, and the dye was covalently coupled according to established procedures.[29-30] The two strands were synthesized and the dye coupled according to established procedures that we have previously described.[17]

Purification and Characterization of Oligonucleotides. All oligonucleotides were purified *via* two rounds of high-performance liquid chromatography (HPLC) on a Shimadzu LC-20AD instrument following our previous studies.[17] The identity of the desired products was confirmed by matrix-assisted laser desorption ionization time-of-flight mass spectrometry (MALDI-TOF) on a Shimadzu Axima Confidence mass spectrometer.

Preparation of Duplex DNA. The oligonucleotides were quantified *via* UV-visible spectroscopy on a Beckman DU-800 UV-Visible spectrophotometer as previously described.[17] The formation of duplex DNA was verified by temperature-dependent absorbance measurements and melting temperature analysis.

Fabrication of Multiplexed Gold Electrode Devices. The chips/substrates featuring multiplexed gold electrodes were prepared from photolithography and metal evaporation as previously described.[30-31]

Self-Assembly of DNA Monolayers. The DNA monolayers were self-assembled onto gold electrode pads from a 5 mM phosphate, 50 mM sodium chloride, pH = 7 buffer solution for 12 h

to 18 h through gold-thiol self-assembly. The substrates were backfilled with mercaptohexanol for 1 h to remove nonspecifically bound DNA and then thoroughly rinsed with the buffer to remove residual mercaptohexanol.

Electrochemistry of DNA Monolayers. The multiplexed substrates were placed in a custom mount (see Supporting Information Figure 1) connected to electrochemical testing hardware (a CH Instruments CHI750D Electrochemical Analyzer and a CHI 684 Multiplexer). The electrochemical measurements were performed in the assembly buffer, then transitioned to 5 mM phosphate, 50 mM sodium chloride, pH = 7 buffer with 4 mM spermidine before introducing various lysates. Square wave voltammetry was recorded with a 4 mV increment, a 25 mV amplitude, and a 60 Hz frequency. The membranes used to separate nuclear lysates from cytoplasmic lysates were the microdialysis strips associated with the Pierce 96-well microdialysis plate, 3.5K molecular weight cutoff (MWCO) from Thermo Scientific.

Square Wave Voltammetry Kinetic Analysis. The electron transfer rates of surface-bound square wave voltammetry were extracted using the method first described by O'Dea and Osteryoung [32] and expanded by our group.[31, 33-34] This kinetic analysis and associated nonlinear curve fitting were performed in Microsoft Excel. Results were reported as means ± standard error (SE) from at least three independent experiments

Results

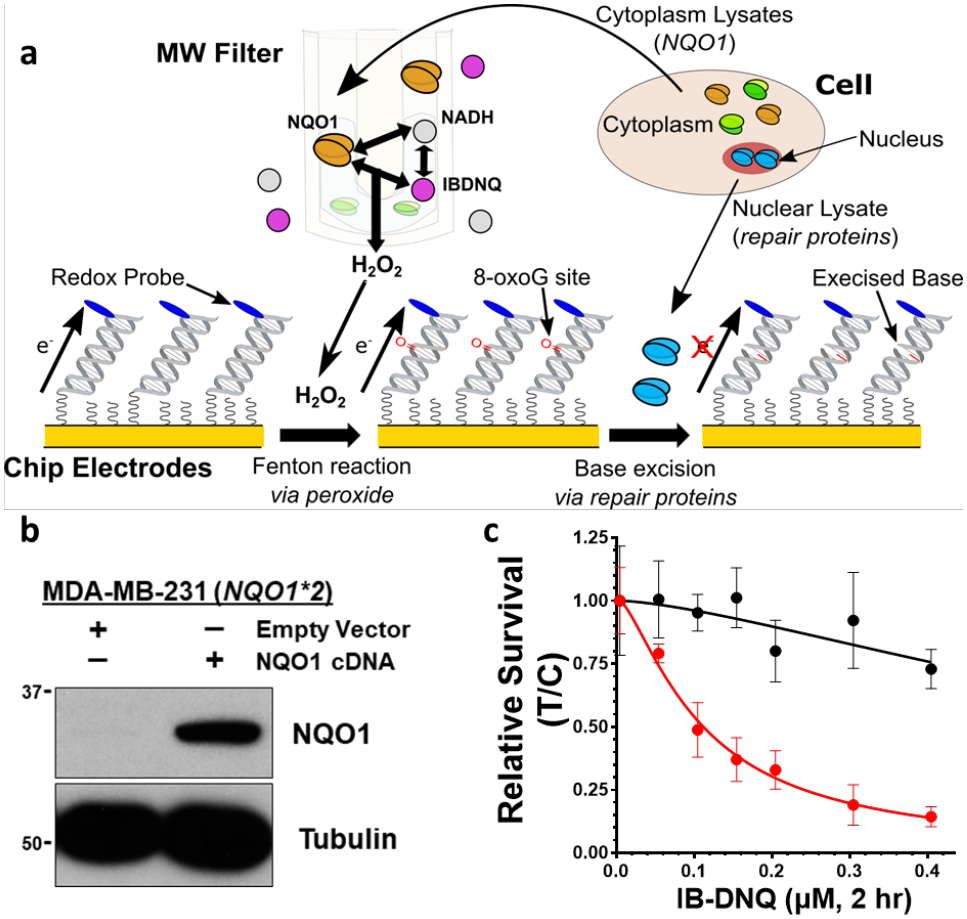

FIGURE 1 a) Concept and cell properties of cell lysate experiments. Nuclear and cytoplasmic lysates are separately collected from cells. A chip with DNA-modified electrodes bearing electrochemically active redox probes is also prepared. Nuclear lysates are added directly to the electrodes, while cytoplasm lysates are added to a molecular weight (MW) filter over the chip that retains large biomolecules but passes small molecules. The IB-DNQ drug and NADH are added to the system, which form a redox cycle with NQO1 that releases superoxide and eventually hydrogen peroxide that passes freely through the filter. Before any damage has occurred, redox-probe labeled DNA monolayers on the electrodes of the chip support electrochemical charge transfer. Hydrogen peroxide from the drug reaction causes oxidative damage to the DNA on the electrodes, and repair proteins from the nuclear lysate remove the damaged base, causing a loss of

the electrochemical signal. b) Western blot depicting NQO1 levels of human triple-negative breast cancer 231 cells with high (NQO1+) and low (NQO1−) expression. c) Relative survival curve of human triple-negative breast cancer 231 cells with high (NQO1+, red data, lower curve) and low (NQO1−, black data, upper curve) NQO1 expression treated for 2 h with various doses of IB-DNQ (n=6). Cultures were allowed to grow for 7-10 days thereafter for colony-forming activity measurements.

Cell Lysate Measurement Concept and Cell Preparation. Our general approach for following IB-DNQ anticancer drug activity in cell lysates is shown in Figure 1 (and Supporting Information Figure S1). Isogenic MDA-MB-231 cells with high NQO1 concentrations (231 NQO1+) and undetectable expression of NQO1 (231 NQO1-) were prepared to establish IB-DNQ as an NQO1-bioactivatable agent (See Supporting Information Figure S2a).[17,23,24] Previous studies have shown that most cancers have aberrant overexpression of NQO1, whereas the corresponding normal tissues have low to undetectable NQO1 enzyme levels.[35] Nuclear and cytoplasmic cell extracts were therefore prepared separately and collected, as it was necessary to ensure similar segregation of proteins and cofactors as accomplished by a cell's nuclear membrane.[17] Each of the lysates was then pipetted into separate areas of a well over a device chip capable of electrochemical reactions through DNA monolayers on electrode surfaces. The cytoplasmic components, which contained NQO1, were added to a 3.5 kDa size-exclusion filter suspended in the well over the chip, which retained proteins but permitted the interchange of small molecules. Nuclear extracts containing repair proteins were added directly to the well solution over the chip. IB-DNQ and NADH (as NADH was anticipated to be lost in lysis) were also added and could freely interchange with each lysate given the low molecular weights. For the NQO1+ cell lysates, NQO1 sequentially

uses NADH followed by IB-DNQ to cycle catalytically and make H_2O_2 reactively—a lethal concentration of IB-DNQ (0.4 μm) generates approximately 3-fold more H_2O_2 relative to vehicle, which was not observed in 231 NQO1-deficient cells (see Supporting Information Figure S2d). This H_2O_2 oxidatively damages the DNA on the electrode surfaces, forming damage products, such as 8-oxoguanine. Repair proteins from the nuclear extracts then remove the damaged bases, causing a lower electrochemical signal on the chip. This approach enables real-time monitoring of electrochemical reactions and control over the specific biological interactions initiated.

Cells for drug study. The cells used to generate lysates for the device study of NQO1 dependent lethality of IB-DNQ were prepared from the triple-negative breast cancer (TNBC) cell line, MDA-MB-231 (231). The cell line has a *2 NQO1 polymorphism and lacked expression of NQO1 protein and enzyme activity (Figure 2).[28] The cell line was corrected for NQO1 expression by lentiviral infection without affecting growth rates *in vitro* or *in vivo.*[28] NQO1+ MDA-MB-231 (NQO1+) or NQO1− MDA-MB-231 (NQO1−) cells were used to examine the lethality of β-lap treatment and for comparison with subsequent chip experiments. Figure 1b shows the expression of NQO1 in each cell sample. NQO1 protein expression is visible in NQO1+ cells while being completely absent in NQO1− cells.

Like β-lap (Bey et al. 2013), IB-DNQ-induced lethality in NQO1+ cancer cells may occur through the rapid generation of superoxide, leading to H_2O_2 formation (Supporting Information Figure 2d) and subsequent large scale DNA damage. NQO1+ and NQO1− 231 cells were treated with various doses of IB-DNQ for 2 h. Cell death happens in an NQO1-dependent manner as 231 NQO1− cells were spared from lethality, while 231 NQO1+ cells showed a 50% lethal concentration (LC_{50}) of approximately 110 nM IB-DNQ (Figure 1c). IB-DNQ killed cancer cells

in an NQO1-dependent manner, and the antitumor activity of IB-DNQ was >10-fold more potent than β-lapachone (ARQ761 in the clinical form).

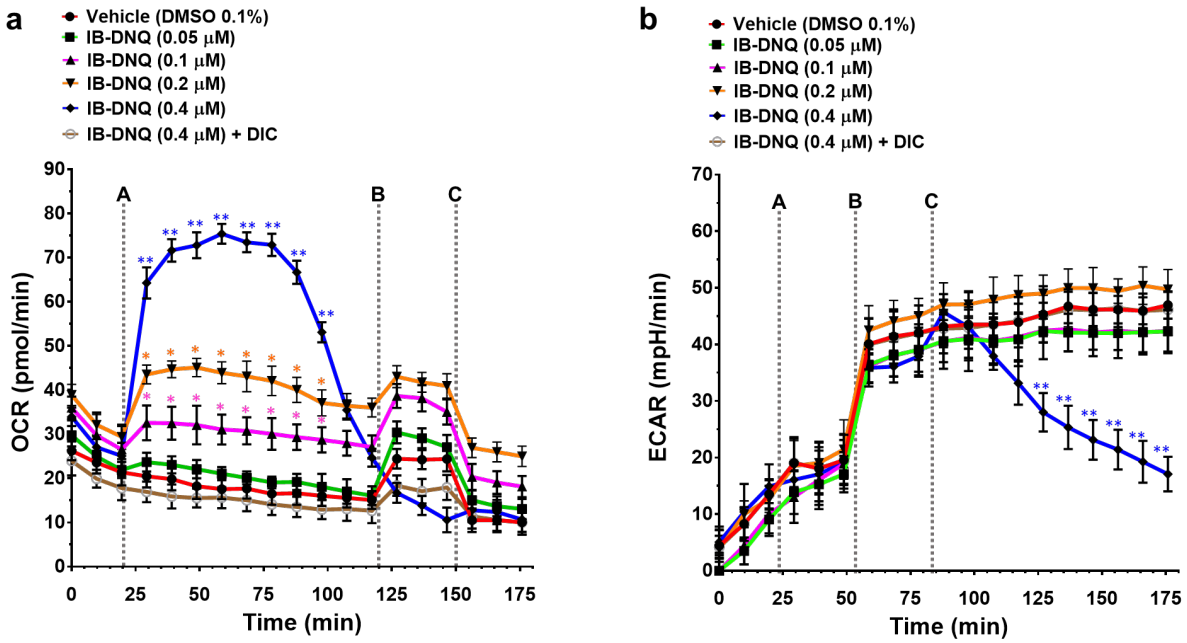

Fig.2: IB-DNQ induces oxidative stress and inhibits glycolysis leading to extensive DNA damage. a) Seahorse analysis of 231 NQO1+ cells assessing oxygen consumption rate (OCR) (n=6) after addition of IB-DNQ, with or without 50 μM dicoumarol (DIC) – a commonly used selective inhibitor of NQO1. IB-DNQ [A] added at t = 20 min, FCCP [B] a protonophore t=120 min, and Rotenone [C] complex I inhibitor t = 150 min. (b) The extracellular acidification rate (ECAR) was measured in 231 NQO1+ (n=6) cells with the addition of glucose [A], oligomycin [B], and IB-DNQ [C] to measure the glycolytic reserve and the role of IB-DNQ in inhibiting glycolysis. Error bars represent mean ± SEM. *$p < 0.05$; **$p < 0.01$ are considered significant compared to vehicle control.

Oxidative Stress and Inhibition of Glycolysis. IB-DNQ treatment (0.05-0.2 μM) resulted in a dose-dependent increase in oxygen consumption rates (OCRs) (Fig. 2a). This suggests that at these doses, IB-DNQ caused significant cell stress, but cells were able to meet

NAD(P)H/NAD(P)+ demand (and avoid higher-order damage response such as PARP1 hyperactivation).[36] At a higher IB-DNQ dose (0.4 μM), the NQO1 futile redox cycle alone becomes exhausted with dramatic decay in OCRs. This OCR effect using the highest dose of IB-DNQ (0.4 μM) is NQO1-dependent because inhibition of NQO1 using Dicoumarol (DIC) (Figure 2a) or the lack of NQO1 (see Supplementary data Figure 2b) showed OCR response almost similar to the vehicle control. The extracellular acidification rate (ECAR) was measured as an indirect analysis of the glycolytic rate of cells with IB-DNQ treatment 231 NQO1+ cells showed reduced ECAR with IB-DNQ (0.4 μM) treatment indicating inhibition of glycolysis as well as a reduction in OCR rates with total NAD(P)H/NAD(P)+ depletion (Figure 2b). As expected, the ECAR effect at 0.4 μM IB-DNQ was also NQO1-dependent as inhibition of NQO1 using Dicoumarol (DIC) (Figure 2b) or the lack of NQO1 (see Supplementary data Figure 2c) showed ECAR response comparable to the vehicle control. NQO1-mediated H_2O_2 levels were produced in the first 2 h of exposure to IB-DNQ as measured (see Supplementary data Figure 2d). These features indicate that lethal levels of DNA damage are occurring near 0.4 μM IB-DNQ.

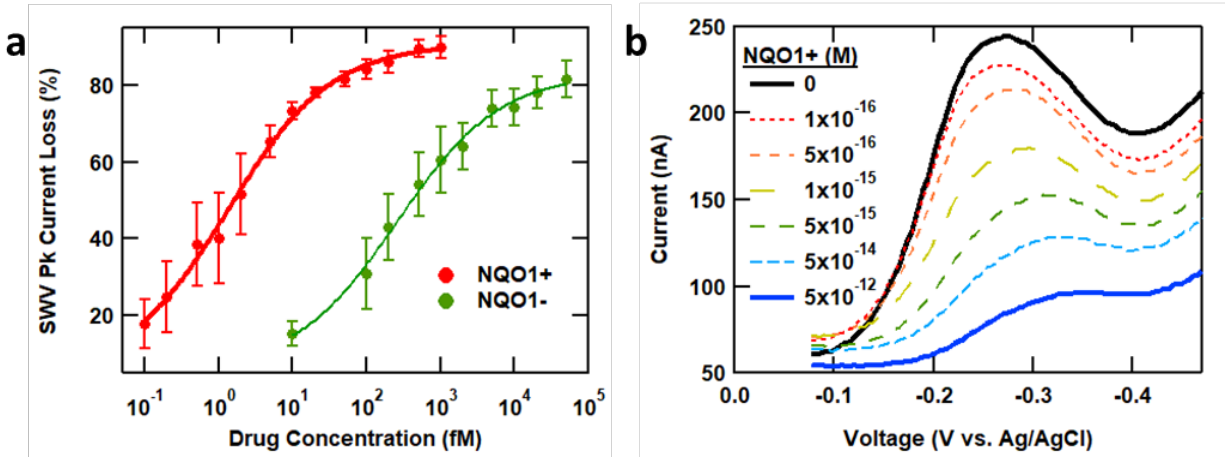

FIGURE 3 IB-DNQ concentration-dependence. a) Square wave voltammetry percent peak current loss after addition of IB-DNQ to chips treated with NQO1 proficient cell lysates (NQO1+) and NQO1 deficient cells (NQO1−). Results are for 3 independent chips of each cell type. Error bars

represent the standard error of the mean. b) An example of the SWV signal from a single electrode in NQO1+ lysates treated with various IB-DNQ concentrations, showing a consistent signal loss.

Device Response at Various IB-DNQ Concentrations. The results of successive addition of IB-DNQ to electrochemical DNA devices under NQO1+ and NQO1− lysates are shown in Figure 3a. Both curves are sigmoidal, indicative of concentration-dependent detection,[37] with the curves significantly offset in concentration. For the NQO1+ curve, IB-DNQ activity is apparent in the 100-200 attomolar (aM) range, with a limit of detection (LOD)[38] of 380 aM. Saturation of damaging activity near 80% signal loss begins at 50 fM levels of IB-DNQ. These features are significantly lower than anticipated, as cell survival assays such as Figure 1c and previous studies have generally identified deoxynyboquinone activity in the nanomolar range,[23-26] but indicate high drug potency and device sensitivity. The NQO1− curve is similar in shape but shifted to higher concentrations by over two orders of magnitude, speaking to the high selectivity of IB-DNQ. Example curves for one DNA electrode in NQO1+ lysates are shown in Figure 3b, revealing the monatomic decrease of SWV peak current with concentration and the highly quantifiable peak current over this range. Supporting Information Figure S3 provides example curves through addition of the lysates and NADH, showing that the redox peak remains stable until addition of the drug, further supporting a drug-specific response.

The NQO1+ and NQO1− curves of Figure 3a were well fit by the Hill equation of the form:

$$S[\beta] = S_0 + (S_M - S_0)\frac{[\beta]^n}{[\beta_{1/2}]^n + [\beta]^n} \qquad (1)$$

where $S[\beta]$ is the SWV signal loss at a particular concentration of IB-DNQ, S_0 is a baseline fit value, S_M is a maximum signal loss value, $[\beta]$ is the IB-DNQ concentration, $[\beta_{1/2}]$ is the IB-DNQ concentration at the midpoint of the signal change, and n is the Hill coefficient. For the NQO1+ lysate curve, $[\beta_{1/2}]$ was found to be 1.3 fM, and n was 0.63, while the NQO1− lysate curve yielded

a [$\beta_{1/2}$] of 254 fM and n of 0.62. The low 1.3 fM midpoint level of the NQO1+ curve again highlights the remarkable drug potency and device sensitivity, whereas the large difference in midpoint values of over two orders of magnitude demonstrates the specificity of the drug and a large therapeutic window. Concerning n, both Hill coefficient values of significantly less than one indicate negative cooperativity—that is, the affinity for the drug reaction decreases with successive reaction events. Likewise, n was 0.62 for the NQO1+ cell survival experiment, thus matching the kinetics from the device and exhibiting its ability to track biologically-relevant activity. This negative cooperativity contrasts the previous study of β-lapachone, which found Hill coefficients of $n = 2.0$, indicating positive cooperativity.[17]

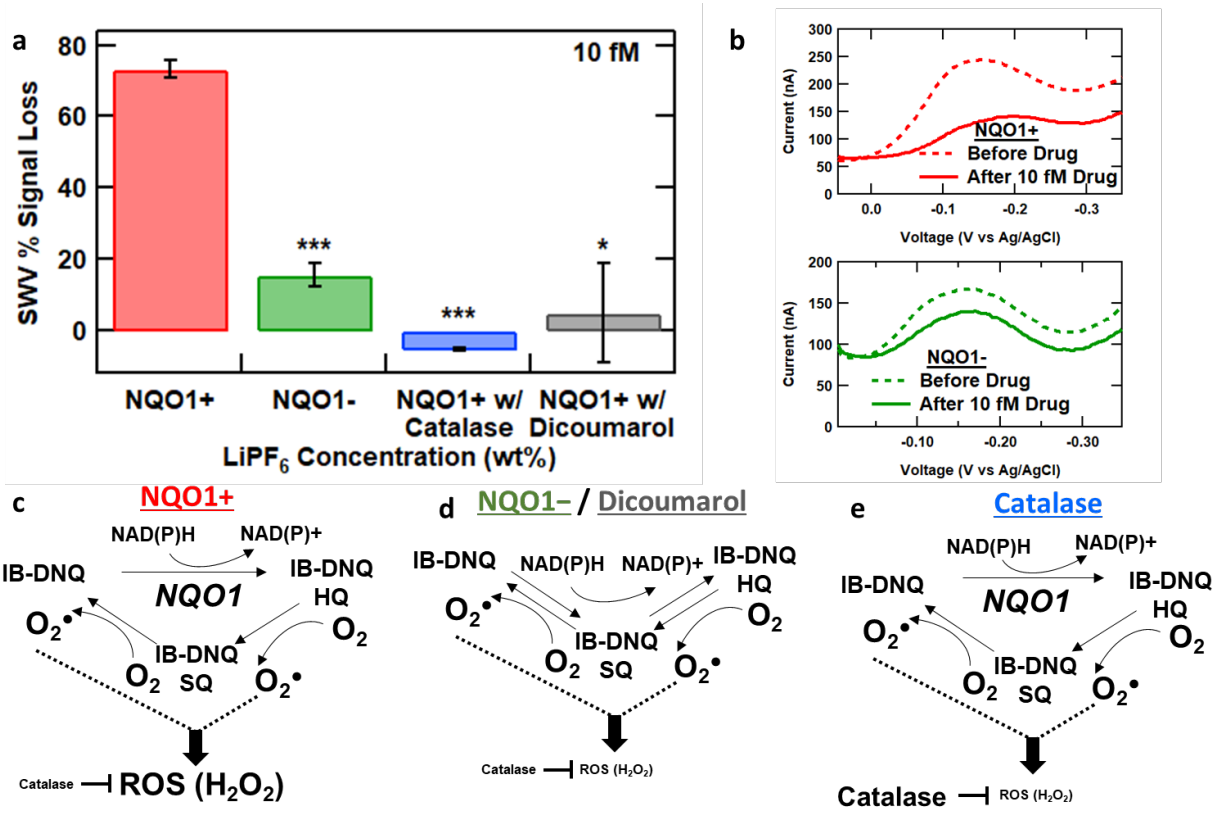

FIGURE 4 Results of cell lysate experiments. a) Square wave voltammetry percent signal loss after addition of 10 fM of IB-DNQ to chips treated with NQO1 proficient cell lysates (NQO1+), NQO1 deficient cells (NQO1−), NQO1+ cells with catalase, and NQO1+ cells with dicoumarol.

Error bars represent the standard error of the mean. Asterisks represent t-test p-values as follows: *p≤0.05; **p≤0.01; ***p≤0.001. b) Example square wave voltammetry before and after 10 fM IB-DNQ treatment in NQO1+ and NQO1− cell lysates. c) Typical reaction cycle for IB-DNQ in NQO1+ cell lysates, showing the catalytic production of H_2O_2 reactive oxygen species (ROS). d) Typical reaction cycle for IB-DNQ in NQO1− and dicoumarol-treated NQO1+ cell lysates. Dicoumarol inhibits NQO1 activity by competitively binding NQO1 and preventing electron transfer with NAD(P)H. e) Typical reaction cycle for IB-DNQ in NQO1+ cell lysates treated with catalase. Catalase abrogates the effects of H_2O_2 by degrading it into H_2O and O_2.

Summary and Controls of IB-DNQ Activity. Figure 4a summarizes the electrochemical device response at 10 fM IB-DNQ in NQO1+ lysates, NQO1− lysates, and NQO1+ lysates coupled with inhibitors of IB-DNQ activity. At this concentration, the devices exhibit a 73.4% SWV peak current loss in NQO1+ cell lysates and only a 15.3% loss in NQO1− lysates, a difference of nearly fivefold. The t-test p-value of less than 0.001 indicates high statistical confidence in this difference. Figure 4b shows example curves from these devices before and after 10 fM addition for each cell lysate, illustrating this differential activity. The IB-DNQ mechanisms under NQO1+ and NQO1− conditions are shown in Figures 4c and 4d, respectively.

Two controls of DNA-damaging activity were also performed in 10 fM IB-DNQ. Catalase is an enzyme that rapidly degrades H_2O_2 into water and oxygen and plays a dominant role in peroxide regulation. Catalase addition abrogates the effects of IB-DNQ by rapidly decomposing the peroxide produced (Figure 4e). The addition of 3nM catalase completely nullifies the impact of IB-DNQ in NQO1+ (Figure 4a). Dicoumarol is a hallmark inhibitor of NQO1 activity,[39-41] acting through competitive binding with NAD(P)H and inhibiting electron transfer to flavin adenine dinucleotide (Figure 4d). Dicoumarol addition at 50 μM considerably lowers the impact of IB-

DNQ in NQO1+ to an average 4.7% signal loss (Figure 4a). Thus, these controls support the DNA-damaging mechanism of IB-DNQ by NQO1-dependent peroxide production.

Finally, a beneficial enhancement of the SWV peak height was often observed for these samples in moving from simple buffer solutions to the biological lysates (see Supporting Information Figure S4). Such a serendipitous increase could indicate either an increase in the fraction of redox-active DNA in the biological solution (typically limited to ~10% of the total surface-bound DNA at room temperature)[34] through the higher ordering of DNA structure or an electrocatalytic increase in the current due to additional redox-active molecules introduced through the biological solution.[42-45] To explore this question, we measured the electron transfer rate using the computational method first described by O'Dea and Osteryoung[32] and expanded by our group[31, 33-34] for surface-bound electrochemistry. Enhancement of the DNA order leads to fast kinetics at or above that found from DNA voltammetry in a buffer, whereas electrocatalysis is assumed to be slower due to the diffusion processes necessary to support redox cycling. Our results showed that a fourfold decrease in the electron transfer rate was observed in going from buffer to biological solution, indicative of the slow, diffusive kinetics associated with electrocatalysis, as well as an approximate tenfold enhancement of the redox-active surface coverage. We will investigate this effect further to gain a greater understanding of the components in our cell lysates that induce this beneficial effect.

Discussion

These experiments highlight the exceptional catalytic cycling activity of IB-DNQ and the precision afforded by this measurement technique. The 380 aM LOD corresponds to a mere 57000

IB-DNQ *molecules* in solution, inducing damage at a rate of approximately 10 million DNA molecules on chip per IB-DNQ molecule. Thus, both the rate of damage by the drug and the sensitivity of the electrochemical technique are noteworthy.

Previously, for electrochemical device measure of the drug β-lap, a high correlation was found between the DNA damage measured on the device and the cell survival rates measured from complete cells. In particular, the β-lap concentration of the midpoint of DNA damage on the chip correlated with that for the onset of cell death, and the β-lap concentration for saturation of DNA damage on the chip correlated with the midpoint of cell death on the cell survival titration curve. However, such a correlation was not observed here with IB-DNQ, which exhibited on-device DNA damage at concentrations of over eight orders of magnitude below that observed for cell survival changes. This likely indicates incomplete cellular uptake of the IB-DNQ through the cellular membrane, a process that is not required for the lysis samples measured on the chip. Indeed, the calculated log P value (an indicator of drug's cell permeability) of IB-DNQ is considerably lower than that for β-lap (−1.69 vs. 1.68), indicating that IB-DNQ is substantially less cell-permeable (see Supporting Information Figure S5). Nevertheless, IB-DNQ is more potent than β-lap, presumably due to its tighter binding to NQO1.[27] Thus, the electrochemical DNA device may identify the damaging potential of emerging drugs and suggest where greater attention to cell permeability is needed.

Conclusions

Electrochemical DNA devices were used to measure the DNA-damaging activity of the NQO1 bioactivatable anticancer drug IB-DNQ in cell lysates derived from 231 NQO1+ and NQO1− cell lines. In NQO1+ cell lysates, IB-DNQ DNA-damaging activity followed the Hill equation with a

limit of detection of 380 aM, a midpoint activity of 1.3 fM, and a saturating activity near 50 fM. IB-DNQ activity similarly followed the Hill equation but shifted to higher concentrations at a midpoint activity of 254 fM. These figures highlight the highly potent and selective nature of IB-DNQ and the sensitivity of the electrochemical biosensing approach. Hill coefficients for device measurements from both NQO1+ and NQO1− lysates were 0.62-0.63 and matched the NQO1+ Hill coefficient of the cell survival experiment, indicating negative damage cooperativity and demonstrating the ability of these devices to capture biological reaction kinetics. At 10 fM drug, activity in NQO1+ lysates was 4.8 times higher than NQO1− lysates and at least 15 times higher than NQO1+ lysates with catalase or dicoumarol (a selective inhibitor of NQO1 activity), confirming the selectivity and NQO1-dependent mechanism of action. The lack of correlation with critical concentrations found in survival assays suggests that IB-DNQ activity is limited by cellular uptake in conventional survival experiments and would be significantly improved with enhanced cellular delivery. Peak currents of the square wave voltammetry signal were serendipitously enhanced in the biological matrix. Kinetic analysis revealed a decrease in electron transfer rate to the DNA-bound redox probe, suggesting that diffusive electrocatalysis was participating in signal transduction. Overall, these results speak to the noteworthy potency and selectivity of IB-DNQ and the high sensitivity and precision of electrochemical DNA devices to analyze DNA-damaging chemotherapies.

Acknowledgments

J.D.S. acknowledges support from the Office of Naval Research grant number N000141612741. This was also supported by NIH/NCI R01CA210489, R01CA221158, and R21CA253645 to E.A.M. The content is solely the responsibility of the authors and does not necessarily represent

the official views of the funders. We thank the group of Leo Bleris at UTD for the low-temperature storage of key experimental components and Dr. Hal Broxmeyer and Dr. Samisubbu R. Naidu at IUSM for providing access and training to Agilent Seahorse XF Analyzer. We also thank Dr. David A. Boothman for his role in establishing this effort, and we dedicate this manuscript in memory of his scientific accomplishments in cancer biology and therapeutics.

Supporting Information

Images of the chip assemblies used for drug studies, western blot, OCAR, ECAR, and relative H_2O_2 levels in various cells and at various drug levels, example SWV curves, drug structures and solubility properties, details of simulations for obtaining kinetic parameters, results of kinetic simulations.

References

1. Cheung-Ong, K.; Giaever, G.; Nislow, C., DNA-Damaging Agents in Cancer Chemotherapy: Serendipity and Chemical Biology. *Chem. Biol.* **2013,** *20* (5), 648-659.
2. Puigvert, J. C.; Sanjiv, K.; Helleday, T., Targeting DNA repair, DNA metabolism and replication stress as anti-cancer strategies. *Febs J.* **2016,** *283* (2), 232-245.
3. Swift, L. H.; Golsteyn, R. M., Genotoxic Anti-Cancer Agents and Their Relationship to DNA Damage, Mitosis, and Checkpoint Adaptation in Proliferating Cancer Cells. *Int. J. Mol. Sci.* **2014,** *15* (3), 3403-3431.
4. Roos, W. P.; Thomas, A. D.; Kaina, B., DNA damage and the balance between survival and death in cancer biology. *Nat. Rev. Cancer* **2016,** *16* (1), 20-33.
5. Labib, M.; Sargent, E. H.; Kelley, S. O., Electrochemical Methods for the Analysis of Clinically Relevant Biomolecules. *Chem. Rev.* **2016,** *116* (16), 9001-9090.
6. Das, J.; Cederquist, K. B.; Zaragoza, A. A.; Lee, P. E.; Sargent, E. H.; Kelley, S. O., An ultrasensitive universal detector based on neutralizer displacement. *Nat. Chem.* **2012,** *4* (8), 642-648.
7. Mousavi, P. S.; Smith, S. J.; Chen, J. B.; Karlikow, M.; Tinafar, A.; Robinson, C.; Liu, W. H.; Ma, D.; Green, A. A.; Kelley, S. O.; Pardee, K., A multiplexed, electrochemical interface for gene-circuit-based sensors. *Nat. Chem.* **2020,** *12* (1), 48-55.
8. Xiang, Y.; Xie, M.; Bash, R.; Chen, J. J. L.; Wang, J., Ultrasensitive label-free aptamer-based electronic detection. *Angew. Chem.-Int. Edit.* **2007,** *46* (47), 9054-9056.
9. Mahshid, S. S.; Mahshid, S.; Vallee-Belisle, A.; Kelley, S. O., Peptide-Mediated Electrochemical Steric Hindrance Assay for One-Step Detection of HIV Antibodies. *Anal. Chem.* **2019,** *91* (8), 4943-4947.

10. Mahshid, S. S.; Ricci, F.; Kelley, S. O.; Vallee-Belisle, A., Electrochemical DNA-Based Immunoassay That Employs Steric Hindrance To Detect Small Molecules Directly in Whole Blood. *ACS Sens.* **2017,** *2* (6), 718-723.
11. Xiang, Y.; Lu, Y., Using personal glucose meters and functional DNA sensors to quantify a variety of analytical targets. *Nat. Chem.* **2011,** *3* (9), 697-703.
12. Baker, B. R.; Lai, R. Y.; Wood, M. S.; Doctor, E. H.; Heeger, A. J.; Plaxco, K. W., An electronic, aptamer-based small-molecule sensor for the rapid, label-free detection of cocaine in adulterated samples and biological fluids. *J. Am. Chem. Soc.* **2006,** *128* (10), 3138-3139.
13. Wu, Y.; Midinov, B.; White, R. J., Electrochemical Aptamer-Based Sensor for Real-Time Monitoring of Insulin. *ACS Sens.* **2019,** *4* (2), 498-503.
14. Shumyantseva, V. V.; Bulko, T. V.; Kuzikov, A. V.; Masamrekh, R. A.; Konyakhina, A. Y.; Romanenko, I.; Max, J. B.; Kohler, M.; Gilep, A. A.; Usanov, S. A.; Pergushov, D. V.; Schacher, F. H.; Sigolaeva, L. V., All-electrochemical nanocomposite two-electrode setup for quantification of drugs and study of their electrocatalytical conversion by cytochromes P450. *Electrochim. Acta* **2020,** *336*, 135579.
15. Porfireva, A.; Vorobev, V.; Babkina, S.; Evtugyn, G., Electrochemical Sensor Based on Poly(Azure B)-DNA Composite for Doxorubicin Determination. *Sensors* **2019,** *19* (9), 2085.
16. Campuzano, S.; Pedrero, M.; Pingarron, J. M., Electrochemical Nucleic Acid-Based Biosensing of Drugs of Abuse and Pharmaceuticals. *Curr. Med. Chem.* **2018,** *25* (33), 4102-4118.
17. Kahanda, D.; Singh, N.; Boothman, D. A.; Slinker, J. D., Following anticancer drug activity in cell lysates with DNA devices. *Biosens. Bioelectron.* **2018,** *119*, 1-9.
18. Boal, A. K.; Barton, J. K., Electrochemical detection of lesions in DNA. *Bioconjucate Chem.* **2005,** *16* (2), 312-321.
19. Boon, E. M.; Ceres, D. M.; Drummond, T. G.; Hill, M. G.; Barton, J. K., Mutation detection by electrocatalysis at DNA-modified electrodes. *Nat. Biotechnol.* **2000,** *18* (10), 1096-1100.
20. Slinker, J. D.; Muren, N. B.; Renfrew, S. E.; Barton, J. K., DNA charge transport over 34 nm. *Nat. Chem.* **2011,** *3* (3), 228-233.
21. Gorodetsky, A. A.; Buzzeo, M. C.; Barton, J. K., DNA-Mediated Electrochemistry. *Bioconjucate Chem.* **2008,** *19* (12), 2285-2296.
22. Lundberg, A. P.; Francis, J. M.; Pajak, M.; Parkinson, E. I.; Wycislo, K. L.; Rosol, T. J.; Brown, M. E.; London, C. A.; Dirikolu, L.; Hergenrother, P. J.; Fan, T. M., Pharmacokinetics and derivation of an anticancer dosing regimen for the novel anti-cancer agent isobutyl-deoxynyboquinone (IB-DNQ), a NQO1 bioactivatable molecule, in the domestic felid species. *Invest. New Drugs* **2017,** *35* (2), 134-144.
23. Huang, X. M.; Dong, Y.; Bey, E. A.; Kilgore, J. A.; Bair, J. S.; Li, L. S.; Patel, M.; Parkinson, E. I.; Wang, Y. G.; Williams, N. S.; Gao, J. M.; Hergenrother, P. J.; Boothman, D. A., An NQO1 Substrate with Potent Antitumor Activity That Selectively Kills by PARP1-Induced Programmed Necrosis. *Cancer Res.* **2012,** *72* (12), 3038-3047.
24. Cao, L. F.; Li, L. S.; Spruell, C.; Xiao, L.; Chakrabarti, G.; Bey, E. A.; Reinicke, K. E.; Srougi, M. C.; Moore, Z.; Dong, Y.; Vo, P.; Kabbani, W.; Yang, C. R.; Wang, X. Y.; Fattah, F.; Morales, J. C.; Motea, E. A.; Bornmann, W. G.; Yordy, J. S.; Boothman, D. A., Tumor-Selective, Futile Redox Cycle-Induced Bystander Effects Elicited by NQO1 Bioactivatable Radiosensitizing Drugs in Triple-Negative Breast Cancers. *Antioxid. Redox Signal.* **2014,** *21* (2), 237-250.
25. Ilcheva, M.; Cao, L. F.; Burma, S.; Boothman, D., Exploiting Isobutyl-deoxynyboquinone-induced DNA damage responses and metabolic changes for breast cancer therapy. *Cancer Res.* **2015,** *75*, P6-02-02.
26. Parkinson, E. I.; Bair, J. S.; Bey, E. A.; Boothman, D. A.; Hergenrother, P. J., Targeting NQO1 as a Potential Anticancer Strategy Using the Small Molecule Deoxynyboquinone. *Eur. J. Cancer* **2012,** *48*, 154-154.
27. Parkinson, E. I.; Bair, J. S.; Cismesia, M.; Hergenrother, P. J., Efficient NQO1 Substrates are Potent and Selective Anticancer Agents. *ACS Chem. Biol.* **2013,** *8* (10), 2173-2183.

28. Pink, J. J.; Planchon, S. M.; Tagliarino, C.; Varnes, M. E.; Siegel, D.; Boothman, D. A., NAD(P)H:Quinone oxidoreductase activity is the principal determinant of beta-lapachone cytotoxicity. *J Biol Chem* **2000,** *275* (8), 5416-24.
29. Gorodetsky, A. A.; Ebrahim, A.; Barton, J. K., Electrical detection of TATA binding protein at DNA-modified microelectrodes. *J. Am. Chem. Soc.* **2008,** *130* (10), 2924-2925.
30. Slinker, J. D.; Muren, N. B.; Gorodetsky, A. A.; Barton, J. K., Multiplexed DNA-Modified Electrodes. *J. Am. Chem. Soc.* **2010,** *132* (8), 2769-2774.
31. McWilliams, M. A.; Bhui, R.; Taylor, D. W.; Slinker, J. D., The Electronic Influence of Abasic Sites in DNA. *J. Am. Chem. Soc.* **2015,** *137*, 11150–11155.
32. O'Dea, J. J.; Osteryoung, J. G., Characterization of Quasi-Reversible Surface Processes by Square-Wave Voltammetry. *Anal. Chem.* **1993,** *65* (21), 3090-3097.
33. Wohlgamuth, C. H.; McWilliams, M. A.; Slinker, J. D., DNA as a Molecular Wire: Distance and Sequence Dependence. *Anal. Chem.* **2013,** *85* (18), 8634-8640.
34. Wohlgamuth, C. H.; McWilliams, M. A.; Slinker, J. D., Temperature Dependence of Electrochemical DNA Charge Transport: Influence of a Mismatch. *Anal. Chem.* **2013,** *85* (3), 1462-1467.
35. Huang, X. M.; Motea, E. A.; Moore, Z. R.; Yao, J.; Dong, Y.; Chakrabarti, G.; Kilgore, J. A.; Silvers, M. A.; Patidar, P. L.; Cholka, A.; Fattah, F.; Cha, Y.; Anderson, G. G.; Kusko, R.; Peyton, M.; Yan, J. S.; Xie, X. J.; Sarode, V.; Williams, N. S.; Minna, J. D.; Beg, M.; Gerber, D. E.; Bey, E. A.; Boothman, D. A., Leveraging an NQO1 Bioactivatable Drug for Tumor-Selective Use of Poly(ADP-ribose) Polymerase Inhibitors. *Cancer Cell* **2016,** *30* (6), 940-952.
36. Gibson, B. A.; Kraus, W. L., New insights into the molecular and cellular functions of poly(ADP-ribose) and PARPs. *Nat. Rev. Mol. Cell Biol.* **2012,** *13* (7), 411-424.
37. B. Esteban Fernandez de Avila, H. M. Watkins, J. M. Pingarron, K. W. Plaxco, G. Palleschi, F. Ricci, *Anal. Chem.* **2013**, *85*, 6593- 6597.
38. D. A. Armbruster, T. Pry, *Clin Biochem Rev* **2008**, *29 Suppl 1*, S49-S52.
39. Scott, K. A.; Barnes, J.; Whitehead, R. C.; Stratford, I. J.; Nolan, K. A., Inhibitors of NQO1: Identification of compounds more potent than dicoumarol without associated off-target effects. *Biochem. Pharmacol.* **2011,** *81* (3), 355-363.
40. Ernster, L.; Ljunggren, M.; Danielson, L., Purification and some properties of a highly dicumarol-sensitive liver diaphorase. *Biochem. Biophys. Res. Commun.* **1960,** *2* (2), 88-92.
41. Ernster, L., [56] DT diaphorase. In *Methods in Enzymology*, Academic Press: 1967; Vol. 10, pp 309-317.
42. Furst, A. L.; Muren, N. B.; Hill, M. G.; Barton, J. K., Label-free electrochemical detection of human methyltransferase from tumors. *Proc. Natl. Acad. Sci. U. S. A.* **2014,** *111* (42), 14985-14989.
43. Furst, A. L.; Muren, N. B.; Hill, M. G., Toward multimarker and functional assays from crude cell lysates: controlling spacing and signal amplification in DNA-CT-based bioelectrochemical devices. *Curr. Opin. Electrochem.* **2019,** *14*, 104-112.
44. Fang, Z. C.; Soleymani, L.; Pampalakis, G.; Yoshimoto, M.; Squire, J. A.; Sargent, E. H.; Kelley, S. O., Direct Profiling of Cancer Biomarkers in Tumor Tissue Using a Multiplexed Nanostructured Microelectrode Integrated Circuit. *ACS Nano* **2009,** *3* (10), 3207-3213.
45. Gasparac, R.; Taft, B. J.; Lapierre-Devlin, M. A.; Lazareck, A. D.; Xu, J. M.; Kelley, S. O., Ultrasensitive electrocatalytic DNA detection at two- and three-dimensional nanoelectrodes. *J. Am. Chem. Soc.* **2004,** *126* (39), 12270-12271.

TOC Graphic

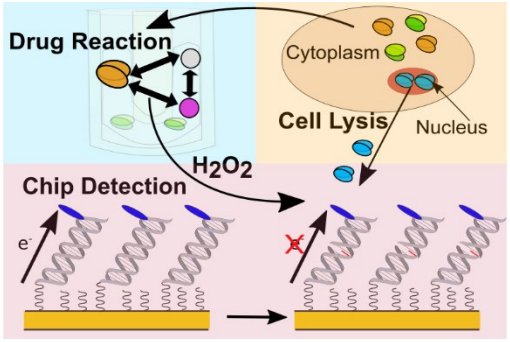
Drug Reaction
Cytoplasm
Cell Lysis
Nucleus
H_2O_2
Chip Detection
e-